PROCESS PLANNING METHOD FOR EXPOSURE CONTROLLED PROJECTION LITHOGRAPHY

Amit S. Jariwala, Harrison Jones, Abhishek Kwatra, David W. Rosen*

George W. Woodruff School of Mechanical Engineering
Georgia Institute of Technology
Atlanta, Georgia, 30332
*Corresponding author. Tel.: +1 404 894 9668 Email: david.rosen@me.gatech.edu

Abstract:

An Exposure Controlled Projection Lithography (ECPL) process with the ability to cure lens shaped structures on transparent substrates is presented. This process can be used to create microlenses and micro fluidic channels on flat or curved substrates. Incident radiation, patterned by a dynamic mask, passes through a transparent substrate to cure photopolymer resin that grows progressively from the substrate surface. A resin response model which incorporates the effects of oxygen inhibition during photopolymerization is used to formulate a process planning method for ECPL. This process planning method is validated for fabricating lens shaped structure on flat transparent substrates using the ECPL system.

1. Introduction

Exposure Controlled Projection Lithography (ECPL) is an additive manufacturing process used to build physical components out of a photopolymer resin. In conventional Stereolithography ("SLA"), a solid object is built layer by layer by exposing successive thin layers of photopolymer resin to a scanned laser beam. Recently researchers including Bertsch et al. [1], Chatwin [2], Monneret et al. [3], Sun et al. [4] and Limaye and Rosen [5] have demonstrated the use of a dynamic mask such as Texas Instruments' Digital Micromirror Device (DMD™) in conventional SLA instead of using a scanned laser beam. Some commercially available machines, such as the Perfactory® range of machines from EnvisonTec, Germany, also use one or more DMD™ chips to pattern the light in a conventional layer-by-layer SLA process [6]. Unlike these processes, ECPL utilizes the dynamic mask such that the irradiation from the DMD™ chip passes through a transparent substrate into a resin vat, and it uses careful control of the light intensity profile to define the vertical shape of the object being fabricated instead of the layer-by-layer approach used in conventional SLA processes. By using a gray-scale image, or alternatively a series of binary bitmap images, both the shape and the intensity profile of the irradiation can be controlled simultaneously; this in turn provides control over the photochemical polymerization reaction in three dimensions. Similar techniques have been investigated by other researchers, in various forms. Erdmann et al. [7] have used mask projection stereolithography through transparent substrates for the fabrication of simple micro-lens arrays, and Mizukami et al. [8] have proposed the use of laser beam scanning through transparent substrates to cure photopolymers for the manufacture of micro-electrophoretic chips. However, to date there is a substantial lack of knowledge with regard to controlling the process in order to achieve the desired accuracy and precision over the final cured parts.

Limaye and Rosen [5] recently proposed a process planning method to control the lateral dimensions of the cured part in a conventional mask-based stereolithography process (then referred to as Mask Projection micro-SLA, or MPμSLA), although the proposed process plan was not intended to precisely control the curing front in the vertical dimension. Jariwala et al. [9] later proposed an elementary process planning method for controlling the cured profile of a thin film cured on a transparent substrate. The process planning method incorporated both a ray tracing model and a basic photopolymerization kinetic model to estimate the required fabrication parameters. Since the process plan was based on a simple polymerization model, the results showed significant deviations in all dimensions. It was hypothesized that the inaccuracies were largely the result of oxygen diffusion and inhibition during the polymerization process. Jariwala et al. [10] subsequently developed a photopolymerization model based on differential equations to model and simulate the effects of oxygen inhibition during polymerization. Although modeling the oxygen inhibition process provided results that more closely matched the observed experimental trends, the model was found inadequate to completely predict the exact shape of the cured part.

In this paper, the chemical reactions occurring during photopolymerization were modeled with revised rate constants. Experiments suggest that the finite element models with revised rate constants can better predict the shape of the cured part. These models were simulated in COMSOL® software package to generate empirical models, which were then used to formulate the process plan. This paper demonstrates a unique process planning approach which involves using iterative chemical simulations to optimize the process inputs required to cure a desired shape from ECPL system.

2. ECPL System

The block diagram of the ECPL process is illustrated in Figure 1. A UV light source is used with a 365nm filter and the light is passed onto the beam conditioning system. The objective of this beam conditioning system is to homogenize the light output from the light source and project it onto the Digital Micromirror Device (DMD™), which is used as a dynamic mask to project grayscale images. The projection system reduces the size of the image projected on the DMD™ and focuses in into the resin chamber. The resin chamber consists of a standard glass microscope slide which acts as a base, an identical glass slide which serves as a top, and spacers of various thicknesses depending on the dimensions of the object to be formed; the liquid photopolymer is placed inside this chamber.

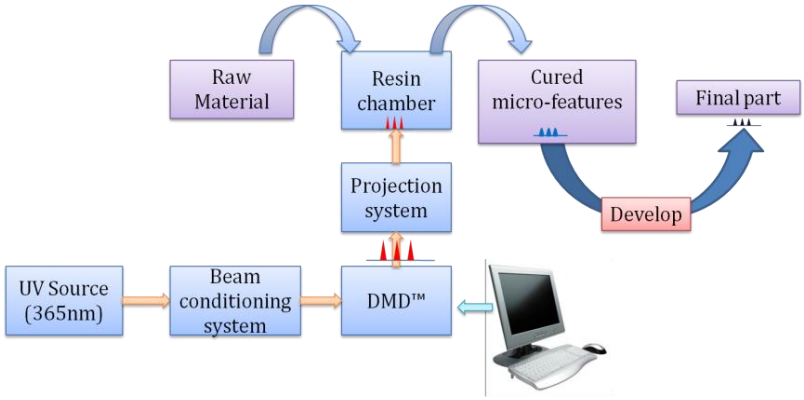

Fig. 1 Block diagram of the ECPL process

Grayscale images are formed on the DMD™ using the computer and projected from the DMD™ into the resin chamber. The regions of the liquid photopolymer resin which receive the irradiation cross-link and are converted into solid polymer, with a vertical profile that roughly matches the intensity profile of the incident light. The uncured monomer is then washed off the cured part in the "developing" process, and the final cured part is obtained on the glass slide. The details of all these modules are explained in Jariwala et al [11]. The discussions in this paper

primarily relate to the chemical reactions occurring within the resin chamber, which consists of two glass slide stuck closely together with a spacer of known thickness placed along two edges as shown schematically in Figure 2. The resin is loaded between this sandwich structure of glass slides and is held by capillary force. The base glass slide acts as the substrate upon which the film is cured.

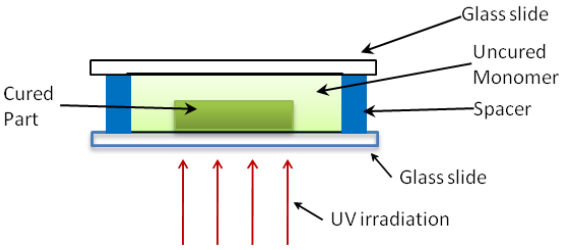

Fig. 2 Schematic of the resin chamber

3.1 Analytical Modeling – Irradiance Model

The ECPL system is analytically modeled in two phases – Irradiance Model and Photopolymerization Model. The irradiance model models the irradiance received by the resin in terms of the process parameters and is presented in detail in Jariwala et al. [12]. The irradiance distribution on the resin depends upon the power distribution across the light beam incident on the bitmap and upon the optical aberrations caused by the imaging lens. This model was experimentally verified by placing a UV-CCD camera at the substrate level (instead of the resin chamber). Figure 3 shows the plot of the exposure profiles from the camera (in dashed lines) superimposed with the simulated exposure profile using the irradiance model (in solid lines). The plots show that the irradiance model based on ray tracing can estimate the actual exposure profile on the substrate level. It is to be noted that there are some deviations from the model, which may be attributed to misalignment of optics, inexact setting of the aperture opening on the system hardware and inexact reproduction of the actual exposure profile on the UV CCD. The resolution of the simulation model was 1μm and that of the UV CCD Camera is ~10μm, which might explain the discrepancy between the experimental and simulation results.

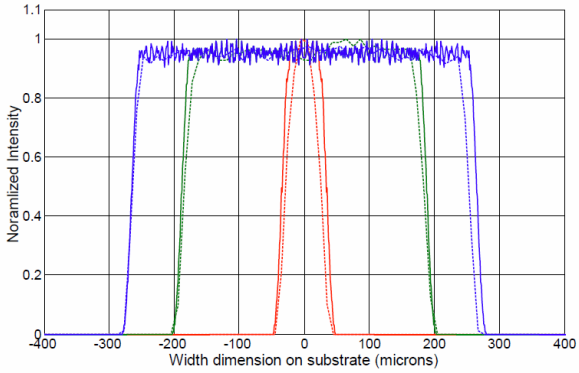

Fig. 3 Comparison of simulation results from Irradiance model (solid lines) with data from Camera (dashed lines). Red corresponds to 10pixels; green to 60pixels and blue to 90pixels

3.2 Analytical Modeling – Photopolymerization Model

Photopolymerization is defined as the reaction of monomers or macromers to produce solid polymeric structures by light-induced initiation and polymerization [13]. Most Stereolithography (SL) resins contain acrylate monomers. For an acrylate resin system, the usual catalyst is a free radical. In Stereolithography, the radical is generated photo chemically. The source of the photo chemically generated radical is a photo initiator, which reacts with an actinic photon. This produces radicals that catalyze the polymerization process. According to Beer Lambert's law of absorption, the exposure (mJ/cm^2) decreases exponentially with depth [14].

$$E(z) = E_{max}\, e^{\frac{-z}{D_P}} \quad (1)$$

where *Dp* is the resin "penetration depth" (a resin parameter) at the given wavelength and E_{max} is the exposure at the surface of the resin ($z = 0$). The cured part height, *z* is shown in Fig. 1 which

shows the schematic of the polymerization process studied in this paper. Based on experimental observations, this model was modified in [3, 4] as follows:

$$z \approx D_{pS} * \ln\left(\frac{D_{pL}}{D_{pS}} * \frac{E}{E_c} + 1 - \frac{D_{pL}}{D_{pS}}\right) \quad (2)$$

The parameters E_c, D_{pL} and D_{pS} are usually fit to experimental data at a specific resin composition and cure intensity. In practice, polymerization does not proceed beyond a limited depth where the exposure falls below a threshold value, E_c. This is primarily due to oxygen inhibition, which imposes a minimal threshold to start polymerization. This exposure threshold model is an oversimplification of the SL process. It directly connects the exposure to the resin and the final solid part shape. It ignores many important intermediate steps. Its ability to predict the three dimensional cured part outline is challenged especially when part resolution is in demand, since it is a one-dimensional model. This shortcoming can be observed by using the empirical polymerization model with the irradiance model.

Test samples were fabricated by projecting lines of varying widths on the DMD™ chip. Specifically, line shaped parts were cured by projecting 30, 60, 90 and 120 micromirrors (or pixels). The UV CCD camera was used to image the intensity profile resulting from projecting the lines, in a similar way in which the plot shown in Figure 62 was obtained. This intensity profile, which is in terms of the gray scale values of the camera, is normalized to obtain the irradiance (energy/time/unit area). The product of irradiance and time is the total incident exposure dose (energy/unit area), 'E'. Eq. 2 was used to predict the shape of the cured part profile for each of the line widths.

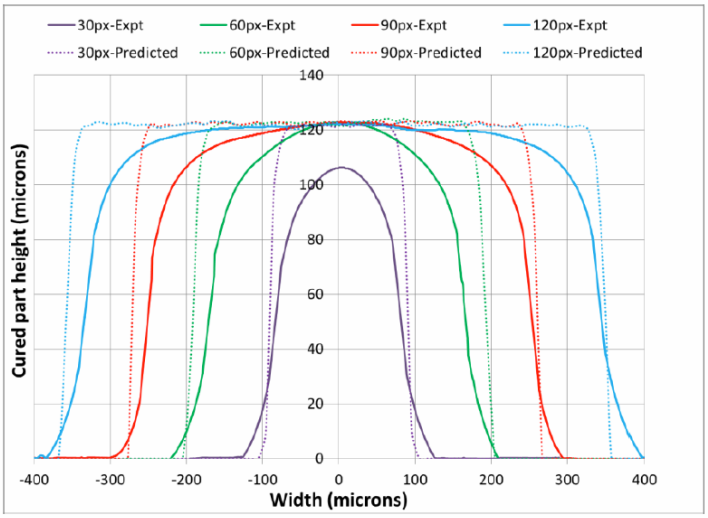

Fig. 4 Plot showing the inadequacy of the existing empirical model to explain the cured part profile. The solid lines show the experimentally observed cured part shapes and the dotted lines depict the predictions using empirical polymerization model

The predicted part profiles are shown as dotted lines in Figure 4. The 3D LEXT Confocal microscope was used to measure the cross-sectional part profile of the cured samples. These profiles are shown as solid lines in Figure 4. It can be seen from the figure that the existing empirical model (which is based on Beer-lambert's attenuation law) fails to explain the presence of a consistent edge curvature. We also notice additional curing beyond the region of exposure close to the substrate. This can be a result of the uncured monomer not being removed due to surface tension between the cured sample and the glass slide, which might have been post-cured and become a part of the previously cured part. However, the primary unanswered question about the polymerization process is – *what causes formation of edge curvature on the cured part resulting from ECPL process*? It is hypothesized that the oxygen inhibition and diffusion might be causing this deviation from the empirical model predictions.

Therefore, the resin kinetic characteristics, as well as the diffusion effects of oxygen which influence the size, shape and properties of parts fabricated by SL cannot be investigated

by using this empirical model. Available chemical models presented in literature only focus on predicting part height and none of them present any approach to predict the shape of the cured profile. We present a unique two dimensional model which can be used to predict part height as well as the shape of the overall cured profile.

The kinetic model for multifunctional acrylate photopolymerization presented here, is based on a set of ordinary differential equations (ODE). The final results show that the kinetic ODE model, based on the critical conversion value, incorporates the impact of process parameters such as initiator concentration, light intensity, oxygen diffusion and exposure time on the final part profile of the object. In addition, the part height predictions from the ODE model are comparable to experiments and the predictions from the modified *Ec–Dp* model.

4. Polymerization Model

4.1 Photopolymerization Kinetics

Recently, Boddapati et al. [15] developed a model to predict the gel time for multifunctional acrylates using a kinetics model. This model incorporated the effects of oxygen inhibition and diffusion in one dimension, which was parallel to the direction of UV irradiation. The rate constants were optimized to fit the experimental data. There were four unique rate constants in the kinetic model, with the diffusivity of oxygen in the photopolymer resin. For ease of reference, the kinetic model is presented as follows. The concentrations of photoinitiator [In], radicals [$R\ \cdot$], unreacted double bonds [DB], and oxygen [O2] were modeled in the kinetic model. The reactions considered by them were as follows [15]. When the photopolymer resin receives light energy, the photoinitiator absorbs it and decomposes into two radicals with first order rate constant of, Kd.

$$In \xrightarrow{K_d} 2R \cdot \tag{3}$$

The initiator decomposition rate K_d is well known in literature and is modeled as a function of the local intensity, which varies with depth (following the Beer-Lambert Law) [16]

$$K_d = \frac{2.3 \emptyset \varepsilon \lambda}{N_A h c} I_0 e^{(-2.3\varepsilon[In]z)} \tag{4}$$

where $0 < \phi < 1$ is the quantum efficiency of the photoinitiator, N_A is Avagadro's number, h is Planck's constant, and c is the speed of light. The molar absorptivity of the resin, ε, depends upon the source wavelength λ. The depth inside the resin is, z. The kinetic equation of the initiator can then be given as,

$$\frac{d[In]}{dt} = -K_d[In] \tag{5}$$

The radicals can then react with the double bonds to form longer chains, or form a dead radical or be quenched with dissolved oxygen as depicted by the following three equations.

$$R \cdot + DB \xrightarrow{K_p} R \cdot \tag{6}$$

$$R \cdot + R \cdot \xrightarrow{K_t} R_{dead} \tag{7}$$

$$R \cdot + O_2 \xrightarrow{K_{t,O_2}} R_{dead} \tag{8}$$

R_{dead} is species produced that destroys one or more radicals. The rate constants used are, K_p for propagation of a radical through an acrylate double bond, K_t for termination between two radicals, and K_{t,O_2} for termination of a radical with an oxygen molecule. R* is non-propogating radicals.

The overall rate of initiator decomposition, R_i , is modeled by multiplying the rate constant K_d by the initiator concentration $[In]$

$$R_i = K_d[In] \tag{9}$$

The kinetic equations for the double bond $[DB]$, live radicals $[R\cdot]$ and oxygen $[O_2]$ can be given as follows:

$$\frac{d[R\cdot]}{dt} = 2k_d I(z)[In] - 2k_t[R\cdot]^2 - k_{t,O_2}[R\cdot][O_2] \tag{10}$$

$$\frac{d[DB]}{dt} = -k_p[R\cdot][DB] \tag{11}$$

$$\frac{\partial[O_2]}{\partial t} = -k_{t,O_2}[R\cdot][O_2] + D_{O_2}\frac{\partial^2[O_2]}{\partial z^2} \tag{12}$$

The effect of oxygen inhibition and diffusion was explicitly modeled in Eq. 12. Due to the high diffusivity of dissolved oxygen in the photopolymer resin, it was assumed that the oxygen would primarily diffuse from uncured top layers of the sample chamber down to the curing front, competing with double bonds for radicals and significantly slowing down the rate at which the double bonds are converted, thus increasing the gel time. This equation was modified to account for oxygen diffusion in two dimensions as shown in Eq. 13.

$$\frac{\partial[O_2]}{\partial t} = -k_{t,O_2}[R\cdot][O_2] + D_{O_2}\frac{\partial^2[O_2]}{\partial x^2} + D_{O_2}\frac{\partial^2[O_2]}{\partial z^2} \tag{13}$$

The researchers estimated the rate constants, K_p, K_t & K_{t,O_2} by fitting the simulation results with the experimental data from FTIR. They had suggested that the individual rate constants are not unique and may vary. Since, the FTIR experiments were conducted at 100 times the intensity of the light used in the ECPL system, it is possible that the effect of oxygen inhibition and diffusion was not adequately captured using the presented rate constants. Hence, these constants were varied to suit the ECPL experimental conditions. The physical parameters, experimental conditions and the fitted rate constants in the study are presented in Table 1.

Table 1 Physical parameters used in this study

Parameter	**Value**	**Units**	**Source**
Quantum efficiency of radical, ϕ	0.6	-	[17]
Molar absorptivity of photons at 365nm wavelength, ϵ	15	m^2/mol	[17, 18]
UV light Intensity, I_0	140	W/m^2	Experimental
Molecular weight of Monomer, TMPTA	296	g/mol	Sartomer
Molecular weight of Photoinitiator, DMPA	256	g/mol	Ciba
Rate constant for propagation reaction, K_p	1.66	m^3/mol-s	Modified from [15]
Rate constant for termination reaction, K_t	1.31	m^3/mol-s	Modified from [15]
Rate constant for termination via oxygen quenching, K_{t,O_2}	125	m^3/mol-s	Modified from [15]
Diffusion coefficient of Oxygen, D_{O_2}	1e-10	m^2/s	[19]
Initial concentration of Oxygen, $[O_2]_0$	1.05	mol/m^3	[20]

The rate constants from the ordinary differential equations are modeled along with diffusion model (chdi) in COMSOL® to estimate the concentration of the individual species at a

given time at a specified location within the resin chamber. The concentration of reactants, especially the monomer concentration [M], during the curing process, can be used to estimate the thickness and profile of the cured part.

Carothers and Flory described a gel as an infinitely large molecule that is insoluble [21, 22, and 23]. Flory used this definition to estimate the degree of cure necessary for the onset of gelation based on the functionality of the reacting monomers [23]. Once the resin starts to gel, the viscosity of the solution increases sharply, and the cure undergoes a rapid transition from a liquid state to a solid state [24]. The degree of cure or the monomer conversion is computed using the following formula. The monomer concentration after polymerization is represented as [M] and the initial monomer concentration is represented as $[M_0]$.

$$Conversion = \frac{[M]-[M_0]}{[M_0]} \tag{14}$$

The shape of the cured part can then be estimated by tracking the coordinates within the sample where the conversion has reached the critical conversion limit. Using the rate constants shown in table 1, a conversion cut-off value of 12%was determined by fitting to the experimental data for TMPTA with oxygen in [16].

4.2. Numerical FE model

COMSOL simulations were conducted to predict the height and profile of the final cured part. The working bitmap, which has a width of 90 pixels, projects an irradiation region which is 560µm wide. A 2D finite element model was created to simulate the experimental conditions. The width of the model was taken as 1mm and the height as 200µm, both of which match the size of the reaction chamber in the actual experimental setup. 1855 triangular elements were used in the simulation. The size of the finest mesh in the irradiation area is 8µm.

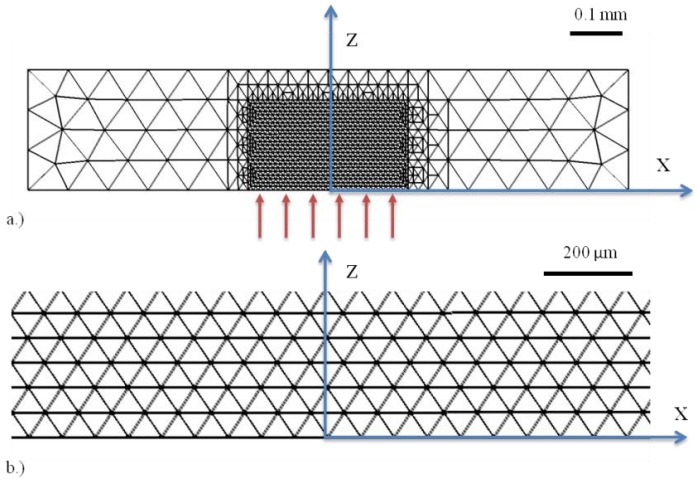

Fig. 5 a.) Schematic of the FE model used in COMSOL; b.) Enlarged view of the FE model

Fig. 5 shows the model of the reaction chamber modeled in COMSOL. The entire rectangular reaction chamber is assumed to be filled with liquid photopolymer. All boundaries are assumed to be insulated, which closely resembles the actual experimental conditions. The coordinate system is also shown in the figure. The boundary between the red arrows shows the region where irradiation is received by the monomer.

4.3. Materials/Chemicals used

For the purposes of this study, we used a tri-functional acrylate monomer - Trimethylolpropane Triacrylate (TMPTA, SR-351) obtained from Sartomer. The photoinitiator 2, 2-dimethoxy-1, 2-diphenylethan-1-one (DMPA, IRGACURE-651) was obtained from Ciba Specialty Chemicals. It should be noted that 125 ppm of Hydroxy Quinone (HQ) or 175 ppm of

Hydroquinone Monomethyl Ether (MEHQ) are included in the monomer formulation of TMPTA to inhibit polymerization from hydroxy radicals while in storage, and the inhibitor was not removed from the experiments, unless specifically noted. The above ppm concentrations are equivalent to the molar concentration of oxygen in the sample, but the exact amount of inhibitor in the monomer at the time of use can vary, and it has been shown that these inhibitors do not impede the photopolymerization as strongly as Oxygen does. All experiments were neat solutions (containing no additional solvent) of TMPTA prepared at near constant initiator concentration of 20% w/w for TMPTA.

4.4. Experimental Validation

The resin in the reaction chamber was cured by the UV irradiation patterned by the bitmaps on DMD™. Experiments were conducted on the ECPL system. The polymerized parts were cured on a glass slide. After curing, the glass slide is removed from the resin chamber and additional uncured resin is removed using an air duster. A 3D laser LEXT confocal microscope was used to measure the cured part profile using the glass slide as the reference.

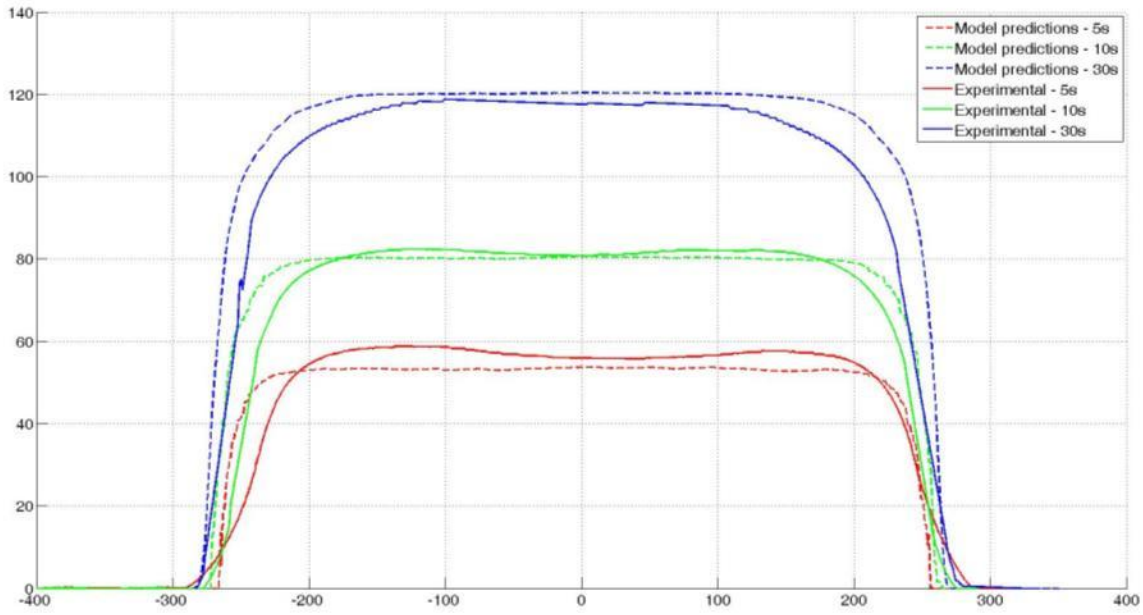

Fig. 6. Comparison of experimental profiles (solid lines) with simulated profiles (dashed lines) Red: 5s exposure; Green: 10s exposure; Blue: 30s exposure. X & Y axes are in micrometers

The experimentally cured profiles were superimposed on the simulated cured profile from COMSOL® simulations as shown in Figure 6. The dashed lines show the predicted profile of the cured part for different energy doses provided. The shape of the cured part was estimated by tracking the coordinates within the sample where the double bond conversion has reached the critical conversion limit of 20%.

The simulations closely predict the height and width of the cured parts. Moreover, the edges also seem to show the curvatures resulting from greater oxygen inhibition effect at the edges than the center. A potential explanation for the mismatch in edge profile is that the rate constants and other coefficients are assumed independent of time and location in the reaction chamber in our study. This assumption needs further in-depth studies, which is beyond the scope

of this paper. A second potential explanation is shrinkage. Shrinkage during resin cure causes reduction in feature dimensions, but it also causes residual stresses, which can lead to distortions in part shapes. Investigation of shrinkage can be a future scope of work, which may be conducted in order to improve the predictability of the model. Despite these limitations, the COMSOL® simulations successfully demonstrate the generation of curved edges for the cured parts. This effect of oxygen inhibition was not considered using the empirical $E_c - D_p$ model. It can only predict that the final cured shape will be the same height and will fail to show the edge curvatures. Hence, the $E_c - D_p$ model, in its original form, cannot be used to predict the shape of the cured part.

5. Process Plan Formulation

The existing process planning methods for ECPL based systems are discussed in literature as presented in Jariwala et al. [9, 12] & Zhao [25]. Through detailed experimentation and error analysis, it was found that the process planning method had several drawbacks. The researchers did not have access to effective metrology tools and hence the experimental validation of their proposed planning methods was not adequate. Moreover, the process-planning algorithm assumed that the complex process of photopolymerization could be assumed as a simple exponential function of exposure (based on the Beer-Lambert law for attenuation). Although the incident exposure (required to cure the photopolymer) can be considered additive, the effect of curing is not necessarily additive in nature. As shown in Section 3.2 and Section 4, the polymerization process is highly coupled and the shape and dimensions of the final cured product depends on the entire exposure pattern and sequence of exposure.

The process-planning problem, as derived from existing literature was split into two parts

i.) Conversion of desired product geometry/shape in to required exposure

ii.) Estimation of required exposure in to process inputs

   a. Estimation of time of exposure for each micromirror
   b. Clustering of micromirrors into bitmaps with common times of exposure

The problem for process planning is to estimate the accurate bitmaps and corresponding exposure time required to cure the desired part shape. This problem can be simplified to a significant extent for the ECPL system studied in this research. The ECPL system can only fabricate structures with monotonically decreasing part geometries, i.e. it is reasonable to assume that the size of the total exposed region should gradually decrease (or remain constant) as more and more height of the cured part is formed. This helps in greatly constraining the optimization problem proposed in the revised hypothesis. Moreover, since the research objective was to fabricate lens like axi-symmetric shapes, the optimization problem can be kept limited to curing two-dimensional axi-symmetric profiles at the center of the substrate.

The overall problem presented by the research question can be simplified as generating the process inputs (a line of clustered micromirrors with corresponding times of exposure) necessary to cure the half-sectional profile of the desired part geometry. Once the line of clustered micromirrors is estimated, the bitmap can be generated by ‘rotating’ the micromirrors along 360° to generate the bitmap. Hence, the process inputs can be listed as follows and illustrated in Figure 7.

B_i – Bitmap used to cure the ith layer, such that L_i is the number of micromirrors offset from the center of the part to be cured and R_i is the total number of micromirrors from the center of the part to be cured.

T_i – Calculated exposure time for ith bitmap

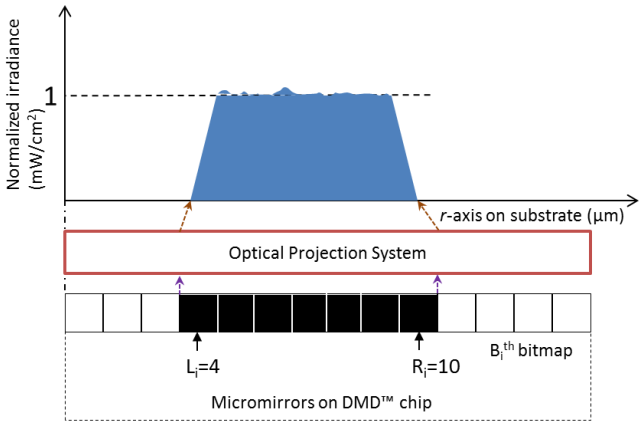

Fig. 7. Illustration of the parameters of the process inputs for the revised process planning

It is to be noted that the first "layer" would be cured on the substrate and hence will not be affected by the previous history of exposure. Hence, estimation of the first group of process inputs (bitmaps and corresponding exposure time) can be made using a pre-calculated material database model based. The process inputs to cure the subsequent "layers" can be estimated using iterative simulations of the chemical kinetic model. Hence, the process planning method can be simplified in form of two-step process as follows:

1. Estimate the first set of process input (bitmap#1 and exposure time) by optimizing the cured part shape using a pre-calculated material database model.
2. Estimate the subsequent process inputs by optimizing the cured part shape using actual simulations of the chemical kinetic model.

5.1 Estimation of first set of process inputs

A material model has to be built such that it incorporates the varying irradiance produced at the edges because of the optical aberrations present in the ECPL system. An irradiation model for the ECPL system was presented in Section 3.1, which was validated using simulations and experiments. This model provided a relationship between the number of pixels exposed on the DMD™ chip and the irradiance produced on the resin substrate. This model was used to create a material database model. An empirical material model (referred to as 'Pixel to cure' database) was created with the conditions as shown in Table 2. The process of estimating the first bitmap is illustrated in Figure 8.

Table 2: Parameters used to create the revised material model ('Pixel to Cure' Database)

Input Variables →	Total exposure time (s)	Number of pixels exposed, R_i
Range →	1 – 30	1 – 45
Increments →	1	1
Output Variables →	Cured Profile, $Z(r)$	Maximum cured part width at base, R

With reference to Figure 8, the first bitmap and exposure time were estimated by optimizing the cured part edge. It is to be noted that the primary function of the first bitmap is not to cure the entire part geometry, but to cure the base and the corresponding edge of the desired part. Hence, the optimization problem is not to be assumed to optimize the entire cured part geometry. Rather, the objective function of the optimization problem is changed based on the resulting cured part height. This explanation can be mathematically explained as follows.

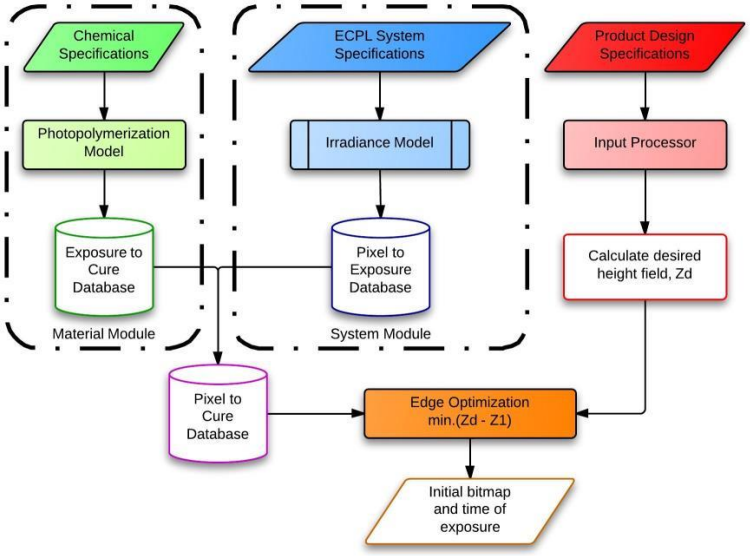

Fig. 8 Flowchart for estimating first set of process inputs

Consider, $Z_d(r)$, as the desired half-sectional cured part geometry, such that r is the radial distance from the center. The variables are illustrated in Figure 9. The edge optimization problem can be written as

Input: Desired cured part geometry: $Z_d(r)$ (μm) (at the substrate level)

Output: Initial bitmap, B_1 and corresponding exposure time, T_1

Objective: $\min\{f(B_i,\ T_i) - Z_{di}(r)\}$, such that $T_i > 0; Ri > Li \geq 0$

where $f(B_i,\ T_i)$ is the cured part geometry obtained from the chemical kinetics' based material model and $Z_{di}(r)$ can be written as follows:

$$Z_{di} = \begin{cases} Z_k = \max[f(B_i, T_i)] & if\ r \leq k \\ Z_r & if\ r > k \end{cases} \qquad (15)$$

such that k is the coordinate of the intersection between the curves Z_k and Z_r along the r-axis (as shown in Figure 7).

It is to be noted that the time increment for each bitmap was limited to 0.1s only, since this is the least possible time increment on the projection system used in the ECPL system studied in this research. Using the above method, the first set of bitmap and its corresponding exposure time was estimated.

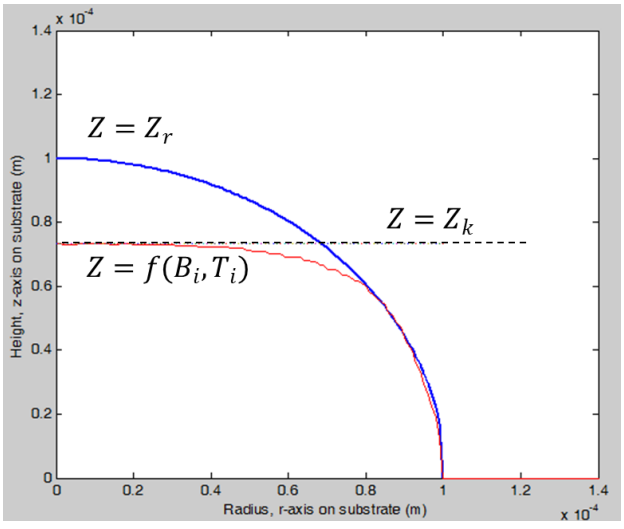

Fig. 9 Variables used in the optimization problem

5.2 Estimation of subsequent set of process inputs

Using the information of the first bitmap and its exposure time, the subsequent bitmaps cannot be estimated directly from the 'pixel to cure' material model. This is because the material model was generated for curing the part on the substrate level and cannot be used directly to estimate the cured part geometry on a previously cured surface. Hence, an optimization method is necessary that incorporates the history (and hence sequence) of curing. Figure 10 shows the flow chart for estimating the subsequent bitmaps and exposure times. The inputs to the flow chart are the first bitmap and exposure time and the desired cured part geometry. The dotted lines show the simultaneous dependence of the optimization module on the system module and the material module. The dashed lines show the iterative nature of the loop and the process stops when the entire desired part geometry is cured completely (within a pre-set threshold).

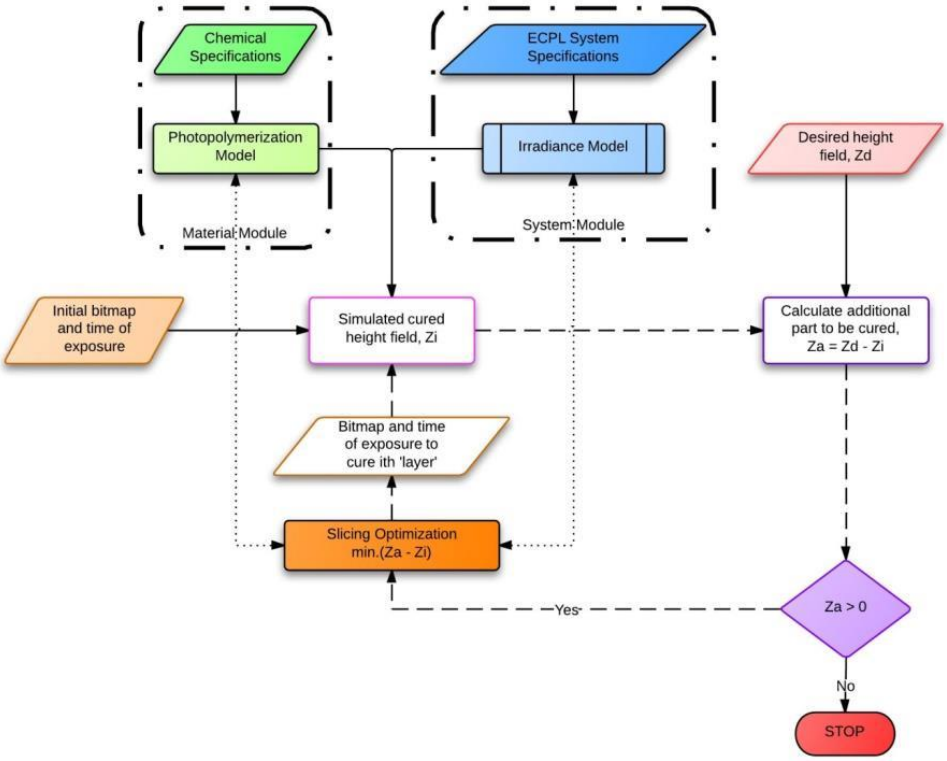

Fig. 10 Flowchart for estimating subsequent set of process inputs

The objective function used in the optimization module for this process is similar to the one explained earlier (in Section 5.1), however the only change is that the simulated cured part is a result of actual chemical kinetics simulations and not a pre-computed material model. The optimization module can be explained as follows.

Consider that the first step (section 5.1) of the process plan resulted in a bitmap, B_1 with parameters, L_1, R_1 and exposure time as, T_1. Since the geometry to be cured is assumed to be monotonically decreasing in width as the height increases, the search space for the parameters of the next bitmap can be set as, $L_2 \geq L_1$; $R_2 \leq R_1$ and $T_2 > 0$. This can be generally denoted as: $L_i \geq L_{i-1}$; $R_i \leq R_{i-1}$ and $T_i > 0$; where *i* is the specific "layer" for which optimization is being conducted. The optimization problem can be expressed as:

Input: Desired cured part geometry: $Z_d(r)$ (μm) (at the substrate level). Initial Bitmap B_1, and time of exposure, T_1.

Output: Bitmaps, B_i and corresponding exposure times, T_i to cure the entire desired part geometry

Objective: $\min\{g(B_i,\ T_i) - Z_{ai}(r)\}$, such that $T_i > 0$; $Ri > Li \geq 0$

where $g(B_i,\ T_i)$ is the cured part geometry obtained from the chemical kinetics' based simulations and $Z_{ai}(r)$ can be written as follows:

$$Z_{ai} = \begin{cases} Z_m = \max[f(B_i, T_i)] - f(B_1, T_1) & if\ r \le m \\ Z_r & if\ r > m \end{cases} \quad (16)$$

such that m is the coordinate of the intersection between the curves Z_m and Z_a along the *r*-axis (similar to 'k', as shown in Figure 9). Z_a is the additional part to be cured and calculated as follows:

$$Z_a = Z_d - Z_i \quad (17)$$

Both the first and second stages of the process plan were coded using Matlab and several example cases were tested. The following sections present the validation to the revised hypothesis using the test cases, both through simulations and experiments.

8. Results and Discussions

In order to validate the process planning method, experiments were conducted on the ECPL system. Matlab scripts were written to encode the revised process planning algorithm. The bitmaps resulting from the process planning method were projected on the DMD™ in the ECPL system for their corresponding times of exposure. The cured samples were then washed, post-cured and measured using the LEXT 3D confocal microscope. The following sub-sections present the results of each sample.

8.1 Test Case – Spherical Lens

The desired part geometry is a spherical lens with radius and sag of 100μm. The resulting 8 bitmaps are shown in Figure 11.

 R_i=12, 7.9s	 R_i=11, 0.8s	 R_i=10, 1.3s	 R_i=9¸1.2s	 R_i=8, 1.8s	 R_i=7, 1.2s
 R_i=6, 1.7s	 R_i=5, 1.8s	X	X	X	X

Fig. 11 Calculated bitmaps and corresponding exposure times for spherical lens example

The simulation result showing the growth of curing process for every individual bitmap projected with the calculated exposure time is shown in Figure 12. Solid black line shows the superimposed desired part profile.

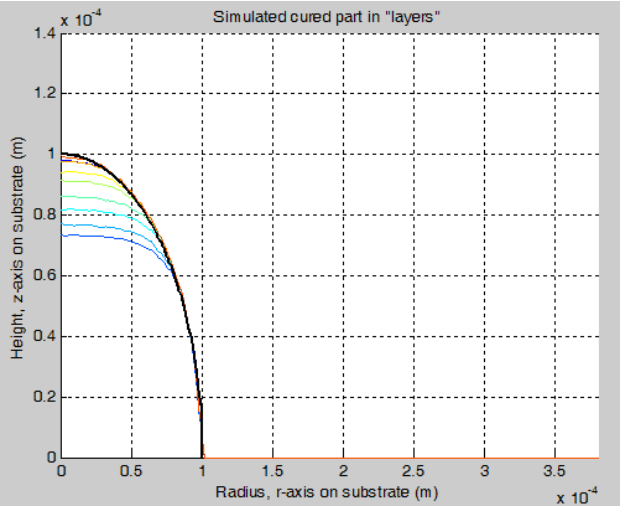

Fig. 12 Simulated half-cross sectional cured part height from individual bitmaps resulting from the process plan

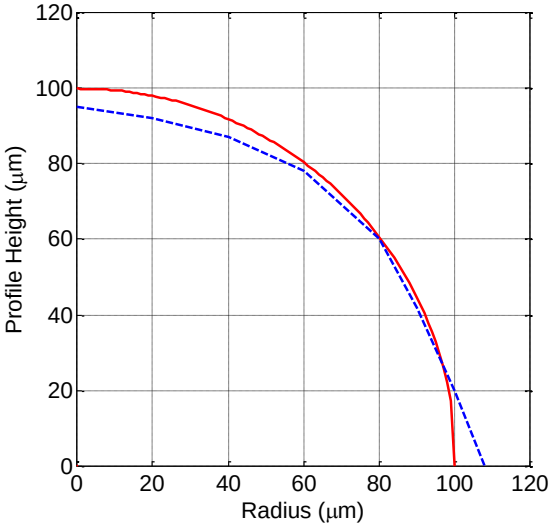

Fig. 13 Comparison of the half-sectional profiles of the cured part sample and the desired part geometry (Desired part profile is in red and experimentally cured profile is shown in blue)

The resin chamber was loaded with the photopolymer and the generated bitmaps were projected on the DMD™ chip for the corresponding exposure times. The sample was then washed and post-cured. Figure 13 presents the comparison between the desired part geometry and the experimentally cured part geometry in a half-sectional view. It must be noted that the experimental curves were obtained by interpolating the measurements of the part heights at approximate intervals of 10μm. It was observed that the experimental samples matched the desired part profile more closely than from the earlier process planning method. The cured part radius (at the base) was larger than desired.

Overall, the sample seems to match the desired part height fairly well. When compared to previously published results [9, 12], it is seen that the revised process planning method yields better results. Moreover, the deviation between the cured part geometry and the desired part geometry is less than 15%, both in sag height and diameter. The under-curing errors are higher for geometries cured with more number of "layers" or bitmaps. Hence, the observed under-curing can be attributed to the errors in accurately projecting the bitmaps using the projector. Post-processing might have been another cause for errors. Based on the experimental results and the simulation results, the process planning method is validated.

It is to be noted that the presented process planning method is currently applicable only for axi-symmetric convex shaped structures. This is adequate for the ECPL system's anticipated end application, which is to fabricate micro-optical components. However, this process planning method can be easily adapted to fabricating non-convex structures (for example, concave lenses) by avoiding the first step and running only the second simulated slicing step. The drawback of avoiding the first step is that the software would take longer to estimate all the bitmaps to cure the desired part geometry, since the starting number of variables will be very large.

9. Conclusions

This paper presented a unique approach to predict the shape of a part cured by photopolymerization. We used two dimensional ordinary differential equations to simulate the

photopolymerization process in order to predict the cured part profile for curing a tri-functional acrylate monomer. These equations incorporated the chemical kinetics and oxygen diffusion and were solved by using COMSOL. The simulated results matched fairly well with the experimental observation for predicting the part height and the overall shape.

The presented model was then used to create the material models to solve the process planning problem. The process planning method was formulated as an optimization problem to obtain the required bitmaps and time of exposure in order to cure the desired shape. The errors on the lateral and vertical dimensions of the cured part formed by using the process planning method were within 15%. Effects of shrinkage should be further investigated to improve the accuracy of the process planning method.

10. References

[1] Bertsch A., Zissi S., Jezequel J., Corbel S. and Andre J., 1997, "Microstereolithography Using Liquid Crystal Display as Dynamic Mask-Generator", *Microsystems Technologies,* **3**(2), pp. 42-47.

[2] Chatwin C., Farsari M., Huang S., Heywood M., Birch P., Young R., Richardson J., 1998, "UV Microstereolithography System That Uses Spatial Light Modulator Technology", *Applied Optics,* **37**(32), pp. 7514-22.

[3] Monneret S., Loubere V., Corbel S., 1999, "Microstereolithography Using Dynamic Mask Generator and A Non-Coherent Visible Light Source", *Proc. SPIE,* **3680**, pp. 553-561.

[4] Sun C., Fang N., Wu D.M., Zhang X., 2005, "Projection Micro-Stereolithography Using Digital Micro-Mirror Dynamic Mask", *Sensors and Actuators A,* **121**, pp. 113-120.

[5] Limaye A. and Rosen D., 2007, "Process Planning Method for Mask Projection Micro-Stereolithography", *Rapid Prototyping Journal,* **13**(2), pp. 76-84

[6] Referred website: http://www.envisiontec.de; visited on 15th July, 2011.

[7] Erdmann L., Deparnay A., Maschke G., Längle M., Bruner R., 2005, "MOEMS-Based Lithography for the Fabrication of Micro-Optical Components", *Journal of Microlithography, Microfabrication, Microsystems,* **4**(4), pp. 041601-1, -5.

[8] Mizukami Y., Rajnaik D., Rajnaik A., Nishimura M., 2002, "A Novel Microchip for Capillary Electrophoresis with Acrylic Microchannel Fabricated on Photosensor Array", *Sensors and Actuators B,* **81**, pp. 202-209.

[9] Jariwala A., Ding F., Zhao X., Rosen D., 2008, "A Film Fabrication Process on Transparent Substrate Using Mask Projection Stereolithography", D. Bourell, R. Crawford, C. Seepersad, J. Beaman, H. Marcus, eds., *Proceedings of the 19th Solid Freeform Fabrication Symposium*, Austin, Texas, pp. 216-229.

[10] Jariwala A., Ding F., Boddapati A., Breedveld V., Grover M. A., Henderson C. L., Rosen D. W., 2011, "Modeling effects of oxygen inhibition in mask-based Stereolithography", *Rapid Prototyping Journal*, **17**(3), pp. 168-175.

[11] Jariwala A., Schwerzel R., and Rosen D. W., "REAL-TIME INTERFEROMETRIC MONITORING SYSTEM FOR EXPOSURE CONTROLLED PROJECTION LITHOGRAPHY," in Proceedings of the Twenty Second Annual International Solid Freeform Fabrication Symposium Austin, Texas, 2011, pp. 99-110

[12] Jariwala, A., Ding, F., Zhao, X., & Rosen, D. W., "A Process Planning Method for Thin Film Mask Projection Micro-Stereolithography", *Proceedings of the ASME 2009 International Design Engineering Technical Conferences & Computers and Information in Engineering Conference.* San Diego, CA, Paper no. DETC2009-87532, 2009.

[13] Decker, C. , "Photoinitiated Curing of Multifunctional Monomers", *Acta Polymer, 43*, pp. 333-347, 1994.

[14] Jacobs, P., "*Rapid Prototyping & Manufacturing: Fundamentals of Stereolithography",* Dearborn, MI., *Society of Manufacturing Engineers*, 1992.

[15] Boddapati A., Rahane S., Slopek R., Breedveld V., Henderson C., and Grover M., "Gel time prediction of multifunctional acrylates using a kinetics model," Polymer, vol. 52, pp. 866-873, 2011.

[16] Boddapati, A., "Modeling Cure Depth during Photopolymerization of Multifunctional Acrylates", M.S. Thesis, Georgia Institute of Technology, School of Chemical & Biomolecular Engineering, Atlanta, 2010.

[17] Tang, Y., "*Stereolithography Cure Process Modeling",* PhD thesis, Georgia Institute of Technology, Atlanta, 2005.

[18] Slopek, R., "In-Situ Monitoring of the Mechanical Properties during the Photopolymerization of Acrylate Resins Using Particle Tracking Microrheology", PhD thesis, Georgia Institute of Technology, Atlanta, 2008.

[19] Li R., and Schork F., "Modeling of the inhibition mechanism of acrylic acid polymerization," Industrial & Engineering Chemistry Research, vol. 45, pp. 3001-3008, Apr 26 2006.

[20] Gou L., Coretsopoulos C., and Scranton A., "Measurement of the dissolved oxygen concentration in acrylate monomers with a novel photochemical method," Journal of Polymer Science Part a-Polymer Chemistry, vol. 42, pp. 1285-1292, Mar 1 2004.

[21] Carothers, W. H., "Polymerization," *Chemical Reviews*, vol. 8, no. 3, pp. 353–426, 1931.

[22] Carothers, W. H., "Polymers and polyfunctionality," *Transactions of the Faraday Society*, 32(1), pp. 0039–0053, 1936.

[23] Flory, P. J., "Molecular size distribution in three dimensional polymers. I. gelation," *Journal of the American Chemical Society*, vol. 63, pp. 3083–3090, 1941.

[24] Winter, H. H. and Chambon, F., "Analysis of linear viscoelasticity of a crosslinking polymer at the gel point," *Journal of Rheology*, 30(2), pp. 367–382, 1986.

[25] Zhao X., "Process Planning for thick-film mask projection micro stereolithography," MS, Mechanical Engineering, Georgia Institute of Technology, Atlanta 2009